*catalysts*

Article

# Improved NOx Reduction Using $C_3H_8$ and $H_2$ with $Ag/Al_2O_3$ Catalysts Promoted with Pt and WOx

**Naomi N. González Hernández [1], José Luis Contreras [1,*], Marcos Pinto [1], Beatriz Zeifert [2], Jorge L. Flores Moreno [1], Gustavo A. Fuentes [3], María E. Hernández-Terán [3], Tamara Vázquez [2], José Salmones [2] and José M. Jurado [1]**

1 Energy Department, CBI, Universidad Autónoma Metropolitana-Azcapotzalco. Av. Sn. Pablo 180, Col. Reynosa, México City C.P.02200, Mexico; iq_naomi@hotmail.com (N.N.G.H.); socram_pinto@hotmail.com (M.P.); jflores@correo.azc.uam.mx (J.L.F.M.) josemanueljuradoflores@outlook.com (J.M.J.)

2 Instituto Politécnico Nacional, ESIQIE. U.P. López Mateos Zacatenco, Mexico City C.P. 07738, Mexico; bzeifert@yahoo.com (B.Z.); avazquezrdz@hotmail.com (T.V.); jose_salmones@yahoo.com.mx (J.S.)

3 Universidad Autónoma Metropolitana-Iztapalapa, CBI-IPH, Mexico City C.P. 09340, Mexico; gfuentes@xanum.uam.mx (G.A.F.); meht4@hotmail.com (M.E.H.-T.)

* Correspondence: jlcl@azc.uam.mx; Tel.: +52-55591911047

Received: 29 June 2020; Accepted: 14 October 2020; Published: 19 October 2020

**Abstract:** The addition of Pt (0.1 wt%Pt) to the 2 wt%$Ag/Al_2O_3$-WOx catalyst improved the $C_3H_8$–Selective Catalytic Reduction (SCR) of NO assisted by $H_2$ and widened the range of the operation window. During $H_2$–$C_3H_8$–SCR of NO, the bimetallic Pt–Ag catalyst showed two maxima in conversion: 80% (at 130 °C) and 91% (between 260 and 350 °C). This PtAg bimetallic catalyst showed that it could combine the catalytic properties of Pt at low temperature, with the properties of $Ag/Al_2O_3$ at high temperature. These PtAg catalysts were composed of $Ag^+$, $Ag_n^{\delta+}$ clusters, and PtAg nanoparticles. The catalysts were characterized by Temperature Programmed Reduction (TPR), Ultraviolet Visible Spectroscopy (UV-Vis), Scanning Electron Microscopy (SEM)/ Energy Dispersed X-ray Spectroscopy (EDS), x-ray Diffraction (XRD) and $N_2$ physisorption. The PtAg bimetallic catalysts were able to chemisorb $H_2$. The dispersion of Pt in the bimetallic catalysts was the largest for the catalyst with the lowest Pt/Ag atomic ratio. Through SEM, mainly spherical clusters smaller than 10 nm were observed in the PtAg catalyst. There were about 32% of particles with size equal or below 10 nm. The PtAg bimetallic catalysts produced $NO_2$ in the intermediate temperature range as well as some $N_2O$. The yield to $N_2O$ was proportional to the Pt/Ag atomic ratio and reached 8.5% $N_2O$. WOx stabilizes $Al_2O_3$ at temperatures ≥650 °C, and also stabilizes Pt when it is reduced in $H_2$ at high temperature (800 °C).

**Keywords:** $H_2$–$C_3H_8$–SCR–NO; $PtAg/Al_2O_3$; bimetallic clusters; $Al_2O_3$–WOx

## 1. Introduction

The conversion of nitrogen oxide emissions (NOx) from diesel machines can be carried out through selective catalytic reduction (SCR) using reductants such as hydrocarbons, alcohols, $NH_3$, $H_2$, and supported metal catalysts [1,2]. The exhaust atmosphere is oxidizing, which hinders the use of three-way technology. Hydrocarbons, present in small amounts in emissions, can be used as a reducing agent to react competitively with $O_2$ or NOx, producing $N_2$, $CO_2$, and $H_2O$ and traces of $N_2O$.

Among the NOx reduction technologies today, urea-based SCR is used in new heavy trucks and some types of cars that run with diesel-type engines. The requirement to add a urea solution into the gas emissions is inconvenient for bus operators and for passenger cars. The possibility of using hydrocarbons to carry out the SCR of NOx (HC–SCR) or alcohols to decrease the contaminants continuously is still attractive [3]. For the SCR of NO using hydrocarbons (HC), catalysts based on Pt, Cu, Ir, Rh, and Ag have been studied [1,2]. The latter metal supported on $\gamma$-$Al_2O_3$ is very interesting because, during SCR using $C_3H_6$ or $C_8H_{18}$, the main product is $N_2$ and not $N_2O$ [2]. It has also been shown to have good stability in the presence of water vapor [4,5] and some tolerance to $SO_2$ [6].

Hydrocarbons have been studied as reducers, but alcohols such as methanol, ethanol, and butanol have also been considered [7–10]. The SCR of NO from $Ag/Al_2O_3$ catalysts in the presence of $O_2$ depends on the concentration and structure of Ag moieties on the surface (i.e., $Ag^+$ cations and $Ag_n$ (n = 8) nanoclusters). $Ag^0$ nanoparticles have been reported to catalyze the total oxidation of hydrocarbons or alcohols to $CO_2$ and $H_2O$ [8]. In studies using reductants such as $C_3H_6$ and impregnation of Ag precursor in $Al_2O_3$, it has been found that there is an optimum concentration in $Al_2O_3$ between 1 and 3 wt% [3,11]. Studies on the nature and role of active Ag species during NOx reduction in the presence of $C_3H_6$ and water have been done, and proposals for reaction mechanisms in the presence of hydrocarbons using spectroscopic techniques have been made [12–24].

There are some drawbacks of the $Ag/Al_2O_3$ catalyst. The main one is that it is active in a narrow range of high temperatures and has low activity below 400 °C in the case of SCR with light hydrocarbons [7,8]. This is an issue because the exhaust gases of lean-burn diesel engines have low temperatures during standard driving conditions.

This problem can be addressed because the operating temperature range has been expanded with the addition of $H_2$ [24–30], which results in the presence of two NO reduction zones: one at low-temperature (80–180 °C) and the other at high temperature (180 to 480 °C). In the search for other reducers, research has also been done using $H_2$ and $NH_3$ together [31,32] and on the coaddition of $NH_3$ and ethanol [33], obtaining good reduction results at low temperatures, although there may be $NH_3$ emissions.

The study of the effect of the hydrocarbon's molecular weight has been carried out using propene and octane [3]. There is one work about the use of gasoline and ethanol as reducing agents [34]. The results showed the presence of $NH_3$, and both NO and ethanol began to react at low temperatures (200–300 °C) on $Ag/Al_2O_3$. Studies with other metals such as $In/Ag/Al_2O_3$–$TiO_2$ using CO showed an improvement in yield to $N_2$ when In was added to Ag [35].

The combined effect of CO and $C_3H_8$ was analyzed, and the temperature window was expanded, but a 5 wt%$Ag/Al_2O_3$ catalyst was required [36]. In this case, the addition of noble metals such as Pt to Ag is useful in obtaining high conversions of NO at low temperatures by using octane as a reduction agent [37]. The catalyst composition showing the highest activity for NOx reduction was a 2 wt%$Ag/Al_2O_3$ doped with 500 ppm Pt. This catalyst showed great capacity for adsorption and partial oxidation of the hydrocarbon, where the Pt has a predominant role.

There have been studies of intermediate storage of NO (passive NOx trap) at low temperatures and regeneration of the adsorbed compound (NO) at high temperatures when the $Ag/Al_2O_3$ catalyst was active to reduce NOx. A $Pt/Ba/Al_2O_3$ catalyst proposed by Tamm et al. [38] in the presence of $H_2$ demonstrated the importance of this to increase the amount of NO stored on the catalyst between 100 and 200 °C. Other noble metals such as the addition of Pd to the $Ag/Al_2O_3$ catalyst [39] showed that the catalytic activity of the catalyst promoted with Pd was higher than the activity of the Ag single metal catalyst in the oxidation of CO and hydrocarbon as well as in reducing NOx.

In another work [40], the Pd–$Ag/Al_2O_3$ catalyst showed higher activity than the $Ag/Al_2O_3$ catalyst at temperatures of 300 to 450 °C. It was found that Pd catalyzed the formation of enolic species, which were converted from $C_3H_6$. The superficial enolic species were quite reactive toward $NO_3-$ and $NO_2$ to form superficial species of –NCO. In the case of the addition of Rh to Ag, theoretical studies have been done that mention the higher capacity of Rh than Ag for NO reduction reactions [41]. Another study of NO reduction where $C_3H_6$, Pt, Rh, and $Ag/Al_2O_3$ were investigated showed that Ag was the most active at higher temperatures, while Pt and Rh were at lower temperatures (200–250 °C) [42].

As has been observed, the SCR of NOx with hydrocarbons (HC–SCR–NOx) has been of great interest until now, because in the presence of an oxidizing atmosphere, as diesel engines work, it is possible to reduce NOx to $N_2$ [24,40]. In the case of Pt catalysts supported in $WO_3/ZrO_2$ and the presence of $H_2$ without Ag for the reduction of NO [43], the authors found high activity at temperatures below 200 °C and high selectivity to $N_2$ (90%). Additionally, the catalyst showed outstanding hydrothermal stability as well as $SO_2$ resistance. Along these same lines, the exceptional stability of WOx has been studied in $Al_2O_3$ and $Pt/Al_2O_3$ [44,45]. It was adopted for the present study, especially to preserve the thermal stability of Pt species', $Ag^0$, $Ag^+$ cations, and $Ag_n$ nanoclusters.

As previously mentioned, the present study contributes to improving the $Ag/Al_2O_3$ catalyst by adding minimal amounts of Pt and WOx in the presence of $H_2$ and $C_3H_8$, which allows for improvement in the SCR of NO. The $PtAg/Al_2O_3$-WOx catalysts were prepared in powder form with the optimal amount of WOx that allows for a high metallic dispersion of Pt and Ag to be obtained, since it is resistant to deactivation by sintering, stabilizing the porous structure of $Al_2O_3$. The study combined $H_2$ and $C_3H_8$ reducers and the presence of small amounts of Pt, which allows for a higher conversion of NO at low temperatures.

## 2. Results and Discussion

Seven Ag and Pt catalysts supported on γ-alumina (with or without WOx) were prepared by the incipient wetness impregnation method with $AgNO_3$ and $H_2PtCl_6$ aqueous solutions. The preparation method is reported in greater detail in the Materials and Methods section. The characterization section is presented first and the catalytic evaluation section later.

### 2.1. Characterization

#### 2.1.1. Textural Properties

The synthesized γ-$Al_2O_3$ (A) presented type IV isotherms, according to the International Union of Pure and Applied Chemistry (IUPAC), the Brunauer Emmett and Teller (BET) area was higher than some commercial alumina with an average unimodal pore diameter of 54 Å (Table 1). The impregnation of Pt as well as Ag and WOx did not significantly modify the area and the other properties.

**Table 1.** Composition of Pt, Ag, and $PtAg/Al_2O_3$ catalysts with 2 wt% Ag and 0.5 wt% W (WOx) prepared in powder. BET area, texture, Pt/Ag atomic ratio, $H_2$ consumption by TPR, and Pt dispersion.

| Catalyst Name | Pt (%) | Ag (%) | Pt/Ag Atomic Ratio | BET Area ($m^2/g$) | Pore Vol. ($cm^3/g$) | Pore Diam. (Å) | $H_2$ Consumption (μmol/$g_c$) | Pt Dispersion (%) |
|---|---|---|---|---|---|---|---|---|
| A | 0 | 0 | 0 | 267 | 0.36 | 54 | 0 | 0 |
| 0.4Pt/A | 0.4 | 0 | - | 256 | 0.36 | 55 | 45.1 | 61 |
| 2Ag/AW | 0 | 2 | - | 264 | 0.38 | 56 | 67 | 0 |
| 0.4Pt/AW | 0.4 | 0 | - | 230 | 0.39 | 68 | 43 | 57 |
| 0.1PtAg/AW | 0.1 | 2 | 0.027 | 226 | 0.37 | 66 | 2.5 | 60 |
| 0.25PtAg/AW | 0.25 | 2 | 0.069 | 218 | 0.36 | 67 | 26 | 46 |
| 0.4PtAg/AW | 0.4 | 2 | 0.110 | 225 | 0.37 | 66 | 41 | 38 |
| 1PtAg/AW | 1 | 2 | 0.270 | 228 | 0.37 | 65 | 112 | 21 |

#### 2.1.2. X-Ray Diffraction (XRD)

The powder x-ray diffraction pattern of all samples showed typical reflections of the g-alumina phase (Figure 1a), with peaks at 2θ = 37°, 46°, and 67°. The presence of another phase was not observed, and the materials were amorphous [46]. According to Aguado et al. [47], these three main peaks correspond to the reflections (311), (400), and (440).

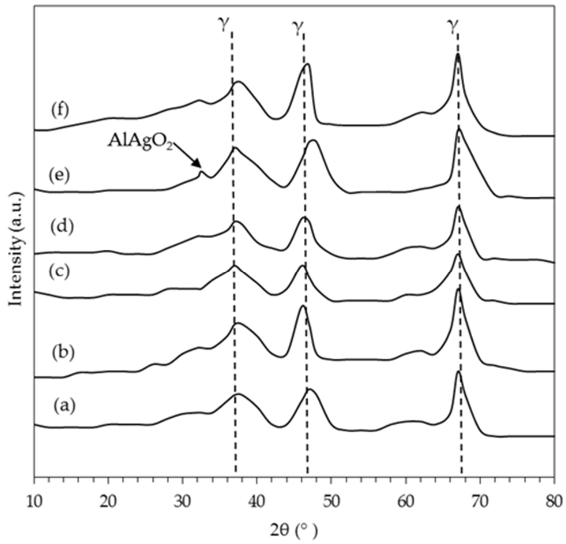


**Figure 1.** X-ray diffraction (XRD) patterns of the catalysts: (**a**) 0.4Pt/AW; (**b**) 2Ag/AW; (**c**) 0.1PtAg/AW; (**d**) 0.25PtAg/AW; (**e**) 0.4PtAg/AW; (**f**) 1PtAg/AW.

Figure 1a–d,f show similar diffractograms of the samples calcined at 500 °C and reduced to 450 °C and no Pt or Ag signals were observed due to their low concentration. However, it was reported that a catalyst of 5 wt%Ag/$Al_2O_3$ showed reflections of metallic Ag [48].

Sample 0.4PtAg/AW (Figure 1e) showed a reflection at 2θ = 38.7°, probably attributed to $AlAg_2O$, however, the other reflections of this compound (2θ = 50.5° and 66.8°) were not noted or revealed the presence of supported $Ag_2O$ particles with a size greater than 5 nm. The broad peaks of these samples showed a stable amorphous and meta structure. The metallic compound $Ag_2O$ has been reported in other studies [49] using Ag concentrations higher than 5 wt%.

### 2.1.3. Temperature Programmed Reduction (TPR)

In the case of 2Ag/AW silver catalyst reduction (Figure 2a), two peaks located at 100 °C and 340 °C was observed, corresponding to the reduction of AgO and $Ag_2O$ clusters. This result has already been reported using a 2 wt%Ag/$Al_2O_3$ catalyst by Bethke and Kung [11] and Maria E. Hernández-Terán [50]. In this last peak, the inflection point or maximum was not observed. These small reduction peaks could be caused by part of the Ag compound already decomposed to metallic silver during calcination [50,51].

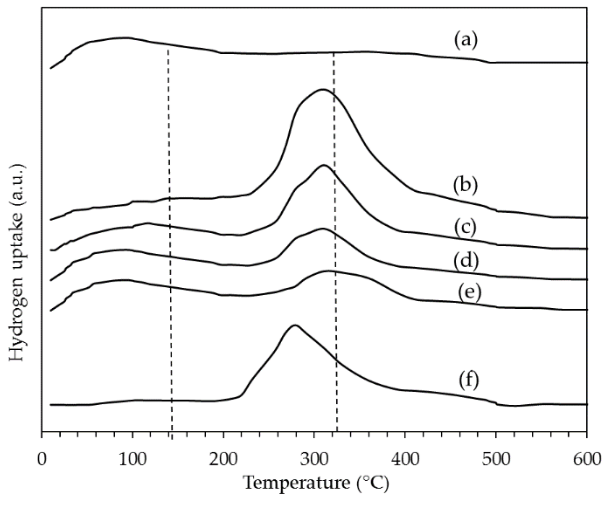


**Figure 2.** TPR of the catalysts: (**a**) 2Ag/AW; (**b**) 1PtAg/AW; (**c**) 0.4PtAg/AW; (**d**) 0.25PtAg/AW; (**e**) 0.1PtAg/AW; (**f**) 0.4Pt/AW catalyst.

In the case of the 0.4Pt/AW catalyst (Figure 2f), the Pt reduction peak could be observed due to the Pt-oxychloride complexes (PtOxCly) located at 280 °C [52]. The $H_2$ consumption for the reduction of (PtOxCly) corresponds to the reduction from $Pt^{+4}$ to $Pt^0$. It is known that the temperature of the reduction peak depends on the precursor of Pt [52]. If a chlorine-free Pt precursor such as $Pt(NH_3)_4(NO_3)_2$ is used, the temperature is close to 70 °C (reduction of $PtO_2$), whereas if $H_2PtCl_6$ is used, the temperature is 290 °C.

In the case of the catalyst with the highest concentration of Pt (1PtAg/AW), two peaks located at 100 °C and 315 °C were observed (Figure 2b). Again, the first corresponded to the reduction of AgO, while the second corresponded to the co-reduction of the two metals' oxides, as has been reported in the literature [50,53]. The maximum peak temperature of this catalyst was 35 °C higher than the peak of the 0.4Pt/AW catalyst (Figure 2f).

This kind of peak has been mentioned in the literature; for example, the Pt–Ag/$SiO_2$ catalyst has been reported as an alloy when Ag is impregnated on the Pt/$SiO_2$ catalyst [54]. It has been found that in such alloys, the Pt and Ag can be secreted by high-temperature oxidation.

The catalysts with lower Pt concentrations (Figure 2c–e) also showed two peaks at temperatures of 100 °C and 305 °C. This last peak was again found at 35 °C higher than the maximum of the 0.4Pt/AW catalyst peak (Figure 2f). The ratio of µmoles of $H_2$ consumed per g of catalyst ($g_c$) for the Pt peaks is shown in Table 1. It was observed that the bimetallic catalysts of PtAg consumed $H_2$ as a function of the concentration of Pt.

In the case of the reduction peak at 100 °C (reduction of AgO), for the 2Ag/AW catalyst (Figure 2a), it was 68 µmol $H_2/g_c$. This value was almost constant for the other values of the reduction of AgO of the bimetallic catalysts since the Ag content was constant (2 wt%Ag), and only in the 1PtAg/AW catalyst did it decrease slightly (Figure 2b).

The ratio of moles of $H_2$ consumed per g of catalyst ($g_c$) for Pt is shown in Table 1. The bimetallic catalysts of PtAg consumed $H_2$ as a function of the concentration of Pt, as reported in the literature [53]. In general, reducing the Pt oxides was completed, while in the case of Ag oxides, it was not completed. Only a part of Ag oxides seemed to be susceptible to reduction, because another part was already in a metallic state after calcination, as has been reported in the literature [50,54].

#### 2.1.4. $H_2$ Chemisorption

The chemisorption of $H_2$ was carried out mainly at the Pt sites. $H_2$ chemisorption of part of the Ag was not observed; even in the case of bimetallic catalysts, it is evident that the consumption of $H_2$ is proportional to the concentration of Pt (Table 1). For the Pt dispersion calculation, the stoichiometry H/Pt was 1, as reported in the literature [55], the dilution state that Ag exerts on Pt atoms is evident, as reported in the literature [53].

In the case of the catalyst with a high Pt content (1PtAg/AW), a large part of the Pt was reduced to metal; however, only a fraction of it remained on the surface of the bimetallic PtAg particles, so it showed a low dispersion (21%). On the contrary, in the case of the catalyst with a low Pt content (0.1PtAg/AW) with a dispersion of 60%, there was a better ratio of surface Pt atoms to Pt atoms in the bulk of the bimetallic. For the 0.25PtAg/AW and 0.4Pt/AW catalysts, there were intermediate Pt dispersions (46 and 38%) that could explain the NO conversion profiles in terms of the activation of $C_3H_8$ and $H_2$.

Some authors have mentioned the presence of a "Pt–Ag alloy" [54]. However, this assertion is doubtful because they did not check if there was a solid solution of Pt and Ag, which is why in our case, we only speak of a bimetallic PtAg system that could have Ag particles decorated with Pt, (or bimetallic core-shell structures), since in all our catalysts, the Ag was always higher in concentration.

On the other hand, there have been studies where the Ag chemisorbs $O_2$, and it has been used to determine its dispersion [56]. The authors validated the stoichiometry of chemisorption of $O_2$ ($O_2$/Ag = 2) by comparing the average particle size using the bright-field TEM, high angle annular dark-field (HAADF), and $O_2$ chemisorption techniques. The active Ag dispersion values they found were: 57.6% (for 1.28 wt%Ag), 51% (for 1.91 wt%Ag), 44.8% (for 2.88 wt%Ag), and 51.2% (for the 6 wt%Ag). The particle sizes were 2.63 nm, 2.62 nm, 3 nm, and 2.63 nm, respectively, at the percentages of Ag, as above-mentioned.

### 2.1.5. SEM of the Catalysts

The calcined 0.4PtAg/AW catalyst showed spherical particles (Figure 3a) that could be related to the presence of $Ag_2O$ [48]. The distribution of particle diameters indicates the predominance (31.64%) of particles of 10 nm, followed by those of 25 and 30 nm (total 42%) (Figure 3b). Finally, those of 50 nm represented 9.9%, and the particles of larger sizes decreased. These results approximate the results reported by Richter et al. [48]. The presence of nanoparticles of different sizes that can vary depending on the type of support has been mentioned. The diameters they found were between 2 to 40 nm with a load of 5 wt%Ag, but predominantly between 5 and 10 nm.

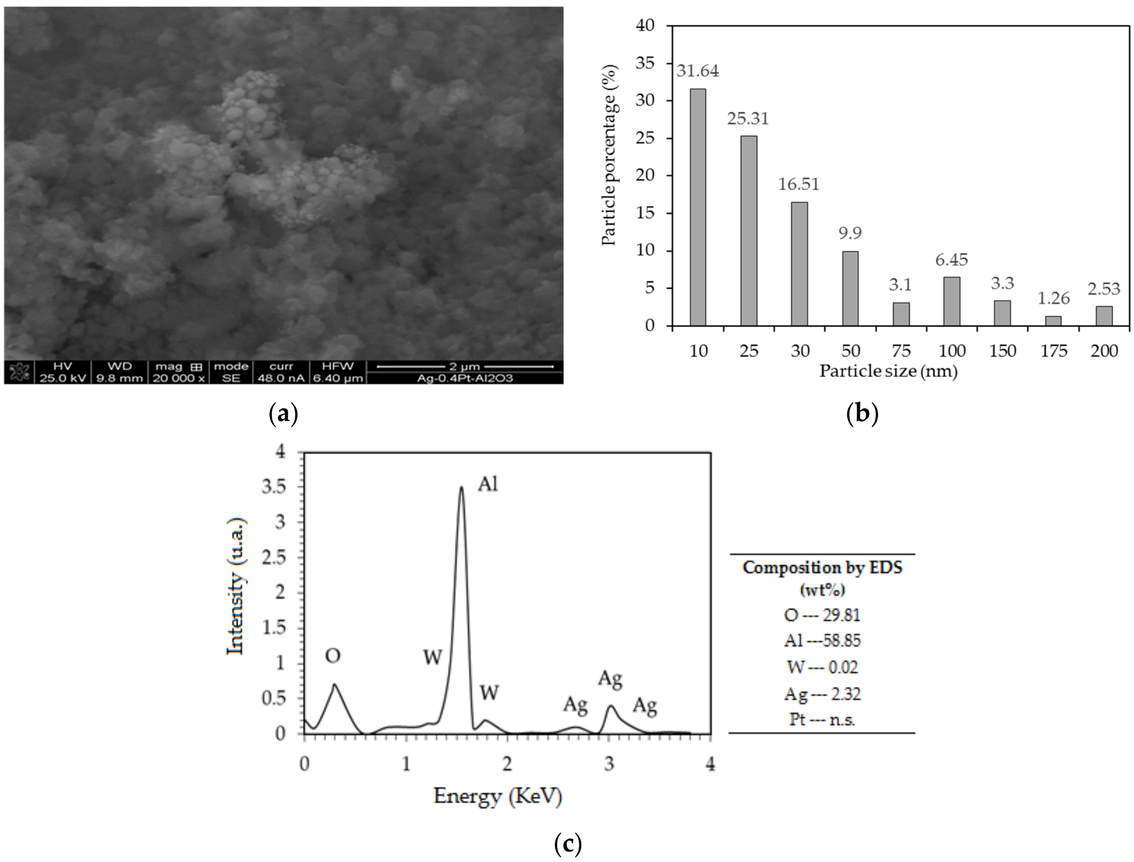


**Figure 3.** Morphological and chemical composition of the catalyst 0.4PtAg/AW calcined at 500 °C. (**a**) SEM micrograph; (**b**) The distribution of particle diameters; (**c**) EDS analysis of the spherical cumulus zone where Pt cannot be analyzed due to its low concentration.

The EDS analysis of the observed area is shown in Figure 3c, where we can observe the presence of Ag and W in amounts approximately at the nominal ones. Richter et al. [48] also identified $Ag_2O$ by convergent beam diffraction, where $Ag_2O$ was indexed, and the primary signal was attributed to it when they were analyzed by temperature-programmed reduction (TPR). The authors found that HAADF was more suitable because the contours of the Ag particles were better distinguished. We also found this problem (Figure 3a) because the particles of Ag showed a dark silhouette that could be confused with part of the alumina support.

Due to the TPR studies, the presence of AgO and $Ag_2O$ is possible, however it was not possible to confirm them by other more advanced techniques. Arve et al. [56] found that both Ag metal and

$Ag_2O$ phases were present in their catalysts, and did not find AgO and cubic $Ag_2O$. The authors concluded that in small particles, $Ag_2O$ is the predominant phase, while metallic Ag is more likely in large particles.

### 2.1.6. UV–Vis Spectroscopy

#### 2Ag/AW catalyst

The existence of different Ag oxidation states was demonstrated by ex situ UV–Vis analysis when the 2Ag/AW catalyst was calcined at 500 °C (Figure 4a). In this case, ionic Ag ($Ag^+$) species were observed showing absorption peaks in the range between 200 and 230 nm [17,49]. The spectrum of the 2Ag/AW sample with a band at 220–235 nm was attributed to the $4d^{10}$ to $4d^9$ $5s^1$ electronic transitions due to highly dispersed $Ag^+$ ions [16,57]. A similar band was observed for the Ag/$Al_2O_3$ and $Ag^+$/H-ZSM-5 catalysts [9,12,30].

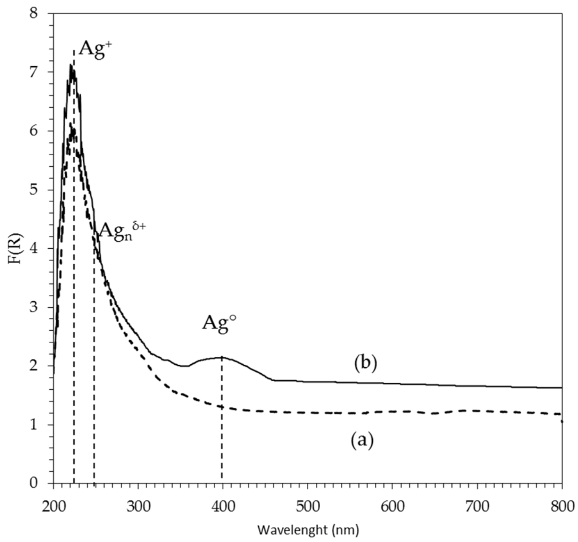


**Figure 4.** Ex situ UV–Vis spectra of the catalysts: (**a**) Calcined 2Ag/AW; (**b**) 2Ag/AW after $H_2$ reduction in a flow of $H_2$ (30 $cm^3$/min) at 500 °C for 2 h (spectrum taken immediately after reduction in $H_2$).

The absorption in the range of 240–288 nm is commonly ascribed to silver nanoclusters $Ag_n{}^{\delta+}$ (n < 8) with a variety of cluster sizes and different oxidation states. After $H_2$ reduction, an absorption band at 340 and 423 nm (Figure 4b) was assigned to larger silver nanoclusters (n > 8) and metallic Ag nanoparticles [16].

#### 0.4Pt/AW Catalyst

The spectrum of the 0.4Pt/AW catalyst calcined at 500 °C showed a band with a maximum at 215–240 nm (Figure 5a). This band was very close to the band found by Lietz et al. [58] at 217 nm for a Pt catalyst prepared by impregnation with $H_2PtCl_6$ in $Al_2O_3$. The authors attributed this signal to a charge transfer band due to the presence of a compound of the type $[PtCl_5OH]^{2-}$, which compares well with the literature data for octahedral $Pt^{4+}$.

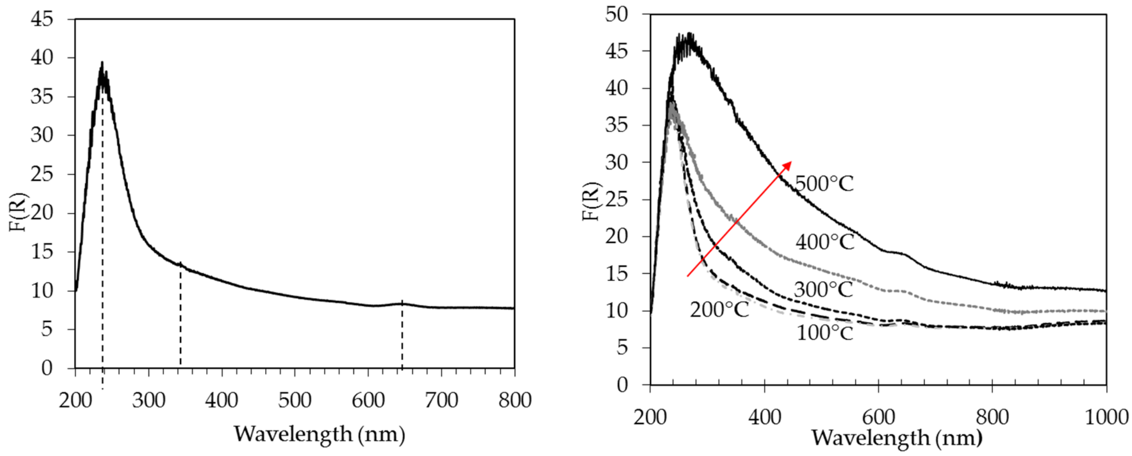


(**a**) (**b**)

**Figure 5.** In situ UV–Vis spectrum of: (**a**) 0.4Pt/AW catalyst calcined at 500 °C; (**b**) 0.4Pt/AW catalyst during the reduction process with 5 vol.% $H_2/N_2$, 0.5 $cm^3$/s.

We found two bands located at 360 nm and 640 nm (Figure 5a). These bands were close with the bands reported by Lietz et al. [58] for a Pt/$Al_2O_3$ catalyst calcined at 500 °C. Their bands were located at 340, 450, and 550 nm, which were associated with the $[PtOxCly]_s$ complexes. We did not find the band located at 450 nm.

The UV–Vis spectra of the 0.4Pt/AW catalyst during the "in situ" reduction with $H_2$ (Figure 5b) showed that with increasing reduction temperature, an increase in the values of the function F(R) corresponding to the band at 320 nm were related to the formation of metallic Pt [58]. During this "in situ" reduction with $H_2$ from 100 °C to 500 °C of the 0.4Pt/AW catalyst, an increase in the F(R) function was observed with respect to the F(R) function of the same calcined catalyst shown in Figure 5a, over a whole spectrum wavelength range from 250 to 1000 nm.

This increase in absorbance due to the reduction of Pt oxychlorocomplexes to metallic particles is responsible for the color change to dark gray of the catalysts. This is related to the so-called color centers [59] and to the appearance of a spectroscopic signal of greater intensity that is due to a greater electronic conduction on the surface of the solid that is associated with the formation of Pt crystallites formed during this reduction process.

PtAg/AW Catalysts

For calcined PtAg/AW catalysts, a band at 220 nm corresponding to $Ag^+$ was observed (Figure 6), as previously reported (Figure 4). This band could also represent the Pt band located at a wavelength of 215–240 nm, which can be attributed to $[PtCl_5OH]^{2-}$ related to octahedral $Pt^{+4}$, as mentioned above. This band was noticeable in the two catalysts with high Pt concentration; 1PtAg/AW and 0.4PtAg/AW (Figure 6a,b), however it did not appear in the two catalysts with low Pt concentration; 0.25PtAg/AW and 0.1PtAg/AW (Figure 6c,d).

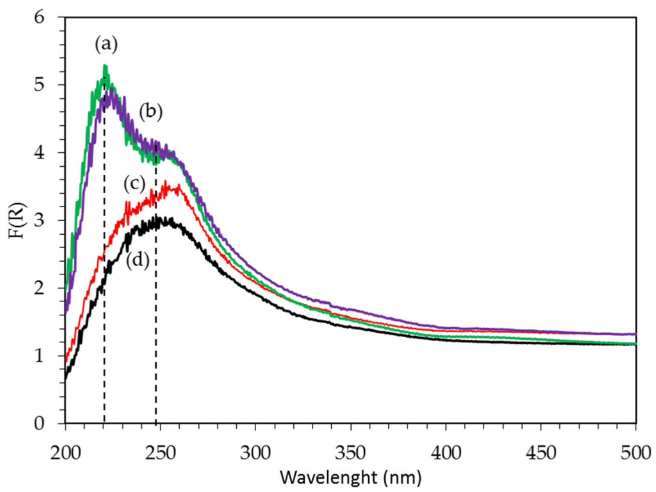


**Figure 6.** Ex situ UV–Vis spectra of the PtAg/AW catalysts calcined at 500 °C when the Pt concentration changed from 0.1 to 1 wt% on $Al_2O_3$–WOx catalysts. (**a**) 1PtAg/AW; (**b**) 0.4PtAg/AW; (**c**) 0.25PtAg/AW; and (**d**) 0.1PtAg/AW.

The broadband with a maximum at 255 nm could correspond to the signal of the Ag metal clusters, ($Ag_n^{\delta+}$), as already mentioned [30]. In this band, the spectroscopic contribution of the signal due to Ag appeared to be higher than the small-signal at 360 nm, as shown by the 0.4Pt/AW catalyst (Figure 5).

## 2.2. Catalytic Activity

### 2.2.1. SCR of NO on Pt and Ag Catalysts

In Figure 7a, the conversion of the 2Ag/AW catalyst started at 370 °C and reached 80% at around 450 °C, followed by a sharp decrease. This reaction temperature window has been previously reported [3,20,30] to be narrow and dependent on the $Al_2O_3$ preparation method [3].

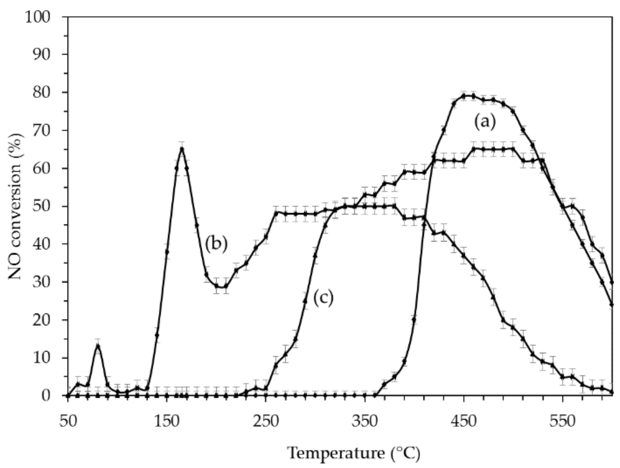


**Figure 7.** $C_3H_8$–SCR–NOx from (**a**) 2Ag/AW catalyst in the absence of $H_2$; (**b**) 2Ag/AW catalyst in the presence of $H_2$; (**c**) 0.4Pt/AW catalyst in the presence of $H_2$. Inlet gas composition: 500 ppm NO, 625 ppm $C_3H_8$, 200 ppm CO, 660 ppm $H_2$, 2 vol.% $O_2$, $N_2$ balance; GHSV = 128,000 $h^{-1}$.

The impregnation method is better than the sol-gel method when the Ag concentration is 2 wt%; if the Ag concentration increases to 5 or 8 wt%, the lyophilized sol-gel method is better. In other words, the method of preparation and the concentration of Ag could provide better catalysts. However, it has been mentioned that the optimal amount of Ag is defined between 1 to 3 wt% [9–11,15,16].

The drawbacks of the $Ag/Al_2O_3$ catalyst behavior when using hydrocarbons as a reducing agent are that the operating temperature window to reduce NO is narrow as well as its low activity below 400 °C. These characteristics do not favor the reduction of NOx emitted by the diesel engines since the temperatures of these emissions are low. Fortunately, when small amounts of $H_2$ are added to the emissions using the $Ag/Al_2O_3$ catalyst, advantages are obtained both in conversion and in the operating window [26].

We could verify this effect when we added small amounts of $H_2$ to our 2Ag/AW catalyst in the flue gas stream (Figure 7b). It was observed that the temperature window in which the catalyst showed activity widened from 130 °C to 500 °C. Additionally, a range of activity appeared at low temperatures (130–200 °C) with medium conversions. The interval from 200 to 470 °C showed better conversions (63%), in agreement with the literature [25–28,30,50].

The reaction interval of 130–200 °C has been the subject of debate on the participation of $H_2$ and the nature of the active species capable of favoring the reaction at low temperatures [27,30]. Studies using Diffuse Reflectance Infrared Fourier Transform Spectroscopy (DRIFTS) of NO and temperature-programmed desorption found two groups of surface NOx species: a less thermally stable group of low temperature (LT) species and a more thermally stable group of high-temperature species (HT). The existence of LT species was attributable to the decomposition of the superficial NOx species formed in the active sites where there is elimination by the addition of $H_2$ or thermal decomposition related to higher oxidation of NO and NOx [27].

The 0.4Pt/AW catalyst in the presence of $H_2$ (Figure 7c) showed a maximum conversion close to 50% at a temperature of 300 °C, starting at 250 °C, and this result coincided with that reported by Lanza et al. [42]. These authors investigated Pt and Rh and found high conversions at low temperature (200–250 °C), showing high selectivity to $NO_2$. On the other hand, when they investigated Ag, a higher temperature was required but with high selectivity to $N_2$. In this study, it was found that the presence of $H_2$ triggered the conversion of NO.

In the case of the SCR of NO on the catalyst with the addition of $H_2$ (2Ag/AW + $H_2$), specifically with 660 ppm $H_2$, a decrease in the light-off temperature down to 150 °C was observed (Figure 7b). This remarkable decrease (from 400 to 150 °C) was similar to that reported by Satokawa et al. [60], and we observed two reaction zones. In the low temperature range (100–180 °C), $H_2$ allows the reactants (or reaction intermediates) to be activated, significantly reducing the activation energy (Ea) of the entire global reaction [48].

According to some authors [48], $H_2$ contributes to reducing oxidized silver species such as $Ag_2O$ to $Ag^0$ on which the nitrate adducts, as above-mentioned, will be adsorbed. The same authors suggest that nano-sized $Ag_2O$ clusters can be reversibly reduced and reoxidized in the presence of $H_2$. These authors also found that the presence of $H_2O$ did not change the Ea. They also found that more adducts or nitrate species were found adsorbed in the presence of $H_2$, and attributed this to a dissociative activation of $O_2$ in the gas phase on the $Ag^0$ particles.

Based on the studies by Azis et al. [27] using DRIFTS and TPD, it appears that there is a formation of stable superficial NOx species that are related to the promoter effect of $H_2$ on the $Ag/Al_2O_3$ catalyst.

#### 2.2.2. SCR of NO with $C_3H_8$ on PtAg Catalysts

The SCR of NO with $C_3H_8$ on the catalyst 2Ag/AW (Figure 8d) in the absence of $H_2$ showed a volcano-like profile that has already been reported [2], where the starting temperature (light-off) was 400 °C with a maximum at 470 °C. The possible presence of monodentate nitrate species at high temperatures is feasible [27]. In contrast, the other bidentate and bridged species that are less stable thermally may not be present.

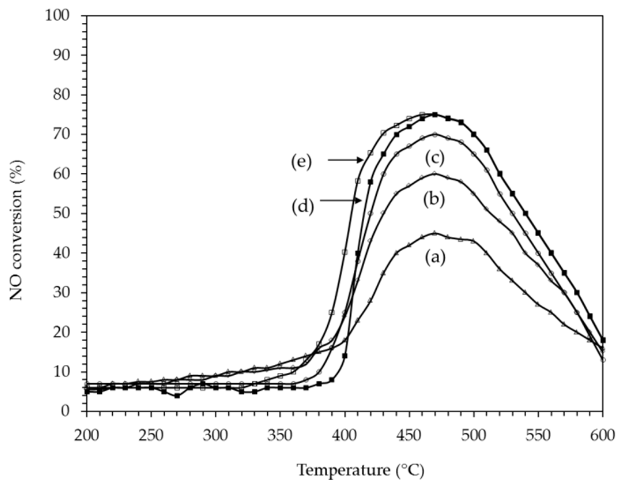


**Figure 8.** $C_3H_8$–SCR–NOx from (**a**) 1PtAg/AW catalyst; (**b**) 0.4PtAg/AW catalyst; (**c**) 0.25PtAg/AW catalyst; (**d**) 2Ag/AW catalyst; (**e**) 0.1PtAg/AW catalyst. Inlet gas composition: 500 ppm NO, 625 ppm $C_3H_8$, 200 ppm CO, 2vol.% $O_2$, $N_2$ balance; GHSV = 128,000 $h^{-1}$.

In general, the addition of Pt to the Ag/AW catalyst did not contribute significantly to the NO conversion at temperatures below 360 °C. In the case of the 1PtAg/AW catalyst (Figure 8a), it only showed a 9% conversion at less than 300 °C. Despite the high Pt content, the NO conversion at 470 °C was the lowest (45%). This behavior indicates that the bimetallic PtAg particles at a Pt/Ag atomic ratio of 0.27 do not provide the best active sites for NO reduction reactions. On the other hand, the Pt dispersion for this catalyst (21%) was the lowest (Table 1). The dilution effect of Pt by Ag seemed evident.

As the Pt concentration decreased in the 0.4PtAg/AW catalyst (Figure 8b) and 0.25PtAg/AW catalyst (Figure 8c), the NO conversion increased to 470 °C, approaching the catalyst conversion of Ag without Pt (Figure 8d). Only when the Pt concentration was less than the 0.1PtAg/AW catalyst (Figure 8e) for a Pt/Ag atomic ratio of 0.027 was the NO conversion slightly higher (75.3%) at 470 °C.

This behavior was similar to that found by Wang et al. [61] for the Pd–Ag bimetallic system. The authors found a 0.01 wt%Pd-5 wt%Ag/$Al_2O_3$ catalyst with higher activity than the 5 wt%Ag/$Al_2O_3$ catalyst. The authors attributed this increase in NO conversion to the presence of enolic species of the type [$H_2C = CH - O - M$], which comes from the partial oxidation of $C_3H_6$ and are highly reactive with NOx adsorbed forming –NCO and –CN. The authors proposed a new reaction mechanism different to that proposed by Burch et al. [2], which helps us explain our results.

It was observed in our catalysts that the 1PtAg/AW catalyst with a high Pt content did not show a high conversion of NO, nor a high dispersion of Pt (Table 1), which suggests that a large part of the total Pt was diluted or covered by Ag atoms, despite showing high $H_2$ consumption values by TPR in Figure 2. It is probable that the addition of Pt (and Pd) to the Ag particles can produce changes of an electronic and superficial type that favor the formation of enolic structures, as demonstrated by Wang et al. [61].

### 2.2.3. $H_2$ Assisted SCR of NO on PtAg Catalysts

The conversion values of NO versus the reaction temperature in the bimetallic PtAg catalysts were dependent on the Pt concentration (Figure 9). The 0.1PtAg/AW catalyst (Figure 9a) with the lowest concentration of Pt showed two high conversion regions (110–180 °C and 180–500 °C), having a maximum conversion of 80% (at 120 °C) and 90% (at 250 °C). The conversion-temperature profile was similar to that shown by the 2Ag/AW catalyst in the presence of $H_2$ (Figure 7b).

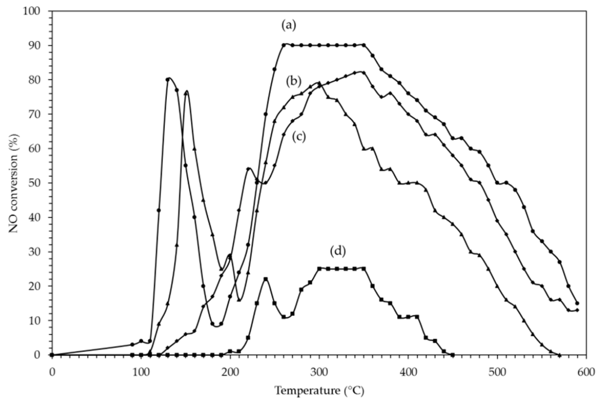


**Figure 9.** Bimetallic catalyst of PtAg for the $C_3H_8$–SCR–NO: (**a**) 0.1PtAg/AW; (**b**) 0.25PtAg/AW; (**c**) 0.4PtAg/AW; (**d**) 1PtAg/AW in the presence of $H_2$. Inlet gas composition: 500 ppm NO, 625 ppm $C_3H_8$, 200 ppm CO, 660 ppm $H_2$, 2 wt% $O_2$, $N_2$ balance; GHSV = 128,000 $h^{-1}$.

The addition of Pt to the 2Ag/AW catalyst showed better conversions and a full temperature window and was also more active at low temperatures (between 100 to 180 °C). These advantages have also been reported in the literature by Gunnarsson et al. [37]. These authors used lower Pt concentrations and reported as optimal a catalyst with 2 wt%Ag plus 500 ppm Pt, which showed the highest activity at low temperature.

The authors attributed this behavior to an ability to adsorb hydrocarbons and partially oxidize them on the surface of bimetallic Pt-Ag particles. The presence of Pt could produce a lower barrier for dissociative hydrocarbon adsorption as well as a change in oxidation potential, which in turn, could be attributed to the Pt doping.

The NO conversions of the catalyst 0.25PtAg/AW (Figure 9b) were 78% (at 150 °C) and 78% (at 300 °C), while when we increased the Pt load in the 0.4PtAg/AW catalyst (Figure 9c), there was perhaps a drop in the NO conversion to 54% (at 220 °C) and 80% (at 330 °C). Finally, when we increased the Pt concentration to 1% with the 1PtAg/AW catalyst (Figure 9d), we observed a low conversion of 22% (at 240 °C) and 25% (at 300 °C).

Additionally, in the low temperature region (100–180 °C), the catalyst with 0.1PtAg/AW showed a maximum conversion of 82% versus the 64% conversion of the 2Ag/AW catalyst (a difference of 18%) (Figure 10a). In the high temperature region (250 to 360 °C), the Pt catalyst showed a maximum conversion of 90% compared to a maximum conversion of 65% without Pt. With these results, it was demonstrated that the addition of Pt in low concentrations improved the activity of the 2Ag/AW catalyst.

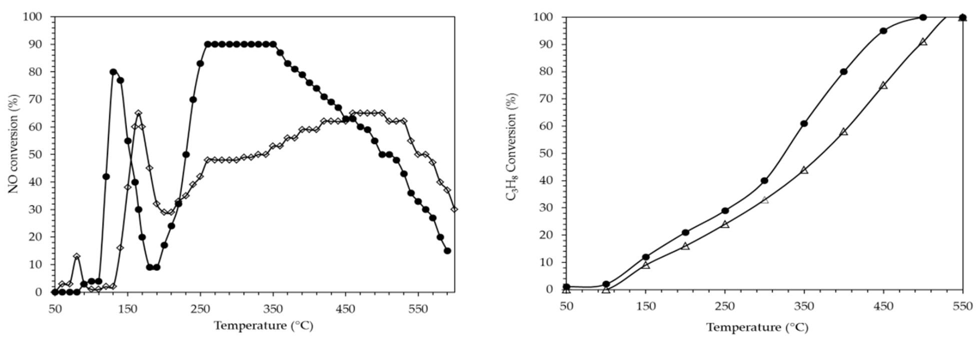


(**a**) (**b**)

**Figure 10.** NO and $C_3H_8$ conversion in the reaction $C_3H_8$–SCR–NO. (**a**) NO conversion with (•) 0.1PtAg/AW and (◊) 2Ag/AW; (**b**) $C_3H_8$ Conversion with (•) 0.1PtAg/AW and (Δ) 2Ag/AW catalysts. Inlet gas composition: 500 ppm NO, 625 ppm $C_3H_8$, 200 ppm CO, 660 ppm $H_2$, 2 vol.% $O_2$, $N_2$ balance; GHSV = 128,000 $h^{-1}$.

During the combustion of $C_3H_8$ in the presence of Ag or (AgPt), we observed the effect of Pt in the presence of Ag clusters (Figure 10b). The $C_3H_8$ conversion for the 0.1PtAg/AW catalyst was found to be higher than the conversion of the catalyst containing only Ag (2Ag/AW). This experimental fact was also reported by Gunnarsson et al. [37]. The presence of Pt in the $Ag/Al_2O_3$ catalyst modified the $C_3H_8$ conversion, (Figure 10b) presenting two regions, with a turning point of the $C_3H_8$ conversion at 300 °C, which was related to the NOx reduction activity where two conversion regions were also observed.

The main factor that allows for the increase in NOx reduction at low temperatures is related to the increase in $C_3H_8$ chemisorption due to the presence of small amounts of Pt on the Ag particles and its corresponding oxidation from NO to $NO_2$.

That is, the Pt–Ag catalyst appears to be able to convert more of the $C_3H_8$ species available on its surface. This phenomenon could be related to a modification of the metallic Ag particles, in terms of both the surface structure and the bulk of their crystal lattice.

Thus, for example, Bordley and El Sayed, [62] prepared Pt–Ag catalysts for electrochemical reactions where the formation of Pt–Ag nano-boxes was reported. They found that the bimetallic particles showed an expanded atomic mesh compared to the Pt atomic mesh. This resulted in the Pt–Ag particles with the least amount of Pt showing improved catalytic activity in the $O_2$ reduction reaction due to a higher binding energy of Pt, which in turn favored an advantageous change in the decrease in the adsorption energy of the intermediates containing oxygen on the surface of these alloyed particles.

According to Gunnarsson et al. [37] the addition of Pt to its $Ag/Al_2O_3$ catalysts produced a greater adsorption of hydrocarbon and with this, an increase in the reduction of NOx at low temperatures. The initial step in the activation of hydrocarbons (such as $C_3H_8$) is known to be the chemisorption and dissociation of a hydrogen atom on the surface of Pt [57].

The dissociation energy of different molecules (or hydrocarbons) present on the surfaces of Ag and Pt is always lower for Pt [49].

During the reaction experiments, the conversion of CO increased from low temperatures to about 375 °C (Figure 11). It was observed that the 0.1PtAg/AW catalyst showed slightly higher conversion than the 2Ag/AW catalyst. These results are similar to those obtained by Shang et al. [36] in terms of CO conversion versus temperature. The authors showed a steep 95% conversion at 200 °C for a 5% $Ag/Al_2O_3$ catalyst. The combustion of both the CO fed to the reactor, and the CO from the combustion of $C_3H_8$ in our case, was carried out in the temperature range from 150 °C to less than 400 °C. Additionally, our results of CO coincided with the study by Gunnarsson et al. [37], in which they found a very low concentration of CO (<5 ppm) at temperatures of 350 °C at the outlet of their reactor for their $PtAg/Al_2O_3$ catalyst.

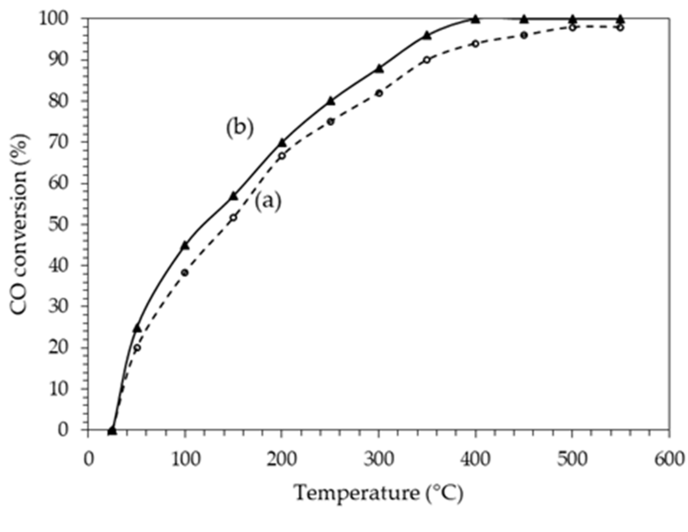


**Figure 11.** CO conversion of catalysts: (**a**) 2Ag/AW and (**b**) 0.1PtAg/AW. Inlet gas composition: 500 ppm NO, 625 ppm $C_3H_8$, 200 ppm CO, 660 ppm $H_2$, 2 vol.% $O_2$, $N_2$ balance; GHSV = 128,000 $h^{-1}$.

The emissions of the nitrogen compounds as a function of the reaction temperature for the 0.1PtAg/AW catalyst are shown in Figure 12. It can be observed that $NO_2$ formed in the interval between 150 to 400 °C (with a volcano-like profile), as has been reported by other authors in the case of $Ag/Al_2O_3$ catalysts [3,30,50] or also $PtAg/Al_2O_3$ [37]. In the latter case, the authors reported the presence of $NO_2$ between 250 to 350 °C.

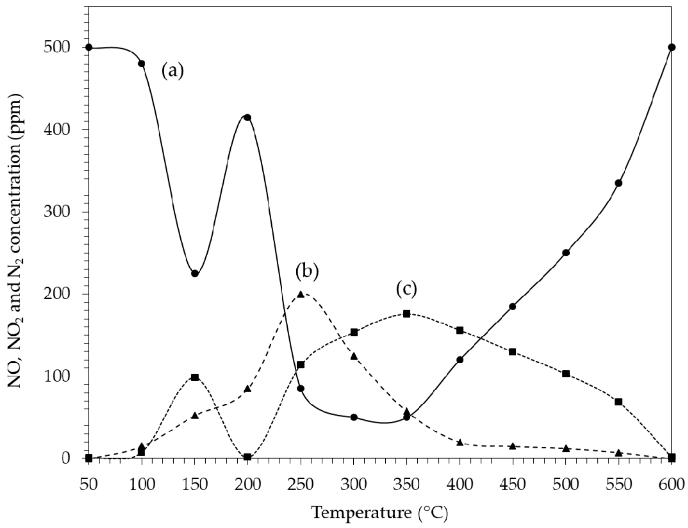


**Figure 12.** Composition of (**a**) NO; (**b**) $NO_2$ and (**c**) $N_2$ (calculated) in the microreactor as a function of temperature during the $C_3H_8$–SCR–NO with the catalyst 0.1PtAg/AW in the presence of $H_2$. Inlet gas composition: 500 ppm NO, 625 ppm $C_3H_8$, 200 ppm CO, 660 ppm $H_2$, 2vol.% $O_2$, $N_2$ balance; GHSV = 128,000 $h^{-1}$.

Between 200 and 350 °C, the $NO_2$ that did not react for the formation of nitrates was being desorbed, as has been reported in the literature [26]. The oxidation of NO with $O_2$ to $NO_2$ is lower than the overall conversion that occurs in the presence of hydrocarbon and NO to $N_2$ [62].

Based on the mass balance of nitrogen compounds at the inlet and outlet of the micro reactor, and Equation (1) proposed by Richter et al. [48], the concentration of $N_2$ at the outlet of the reactor (Figure 12) can be calculated as follows:

$$[N_2] = \frac{1}{2}\,[[NO]_o - [NO] - [NO_2] - 2[N_2O]] \quad (1)$$

where $[N_2]$ is the calculated concentration of $N_2$ (mol/L); $[NO]_o$ is the initial concentration of NO (mol/L); [NO] is the present concentration of NO (mol/L); $[NO_2]$ is the present concentration of $NO_2$ (mol/L); and $[N_2O]$ is the present concentration of $N_2O$ (mol/L).

The decrease in $NO_2$ at 250 °C is related to the partial oxidation of $C_3H_8$, as can be seen in Figure 10b. The formation of $N_2$ showed a maximum at 350 °C and then decreased as a result of the parallel and series reactions that were being carried out.

These bimetallic catalysts produced $N_2O$ at several temperatures. The results of the formation of $N_2O$ in our study are shown in Table 2, and expressed in $Y_{N2O}$ yield, which is defined as $Y_{N2O} = 2 \times [N_2O]/[NO]_o \times 100$. These yields ($Y_{N2O}$) are reported for two temperatures: 200 °C and 400 °C.

**Table 2.** $N_2O$ yield (%) of the PtAg/AW catalysts in $C_3H_8$–SCR of NO with $H_2$.

| Catalyst | Pt/W Atomic Ratio | $Y_{N2O}$(%) at T(°C) | |
|---|---|---|---|
| | | 200 | 400 |
| $Ag/Al_2O_3$ | 0 | 7 | 5 |
| 0.1PtAg/AW | 0.027 | 8.5 | 6.5 |
| 0.25PtAg/AW | 0.069 | 9 | 6.5 |
| 0.4PtAg/AW | 0.11 | 12 | 7 |
| 1PtAg/AW | 0.27 | 14 | 6 |

The results at 200 °C showed that the 2Ag/AW catalyst produced a 7% yield to $N_2O$ while the 0.1PtAg/AW catalyst showed a 8.5% yield at the same temperature. For the 0.25Pt/AW catalyst, the $N_2O$ yield was 9%, which was very similar to that observed for the 0.1PtAg/AW catalyst. In the case of 0.4PtAg/AW and 1PtAg/AW catalysts, the yields were 12.5 and 14%, respectively.

We observed that the formation of $N_2O$ was greater at 200 °C than at 400 °C, as has been found by Shaieb et al. [25]. It was also observed that the formation of the Pt–Ag bimetallic was so strong, probably in the form of the Pt–Ag alloy [54], that Ag decreased the selectivity of Pt to produce $N_2O$, as observed by Gunnarsson et al. [37] when studying catalysts of 2%Ag–0.05%Pt/$Al_2O_3$ in this reaction.

In the case of the 2%Ag/$Al_2O_3$ catalyst (without Pt), other authors such as Meunier et al. [14] reported an 8% yield of $N_2O$ at 450 °C; Richter et al. [48] reported a 2.25% $N_2O$ yield at 267 °C; and Shaieb et al. [25] reported a 6% $N_2O$ at 200 °C. Hernandez and Fuentes [30] reported 1% $N_2O$, Kannisto et al. [3] reported 1.6% at 250 °C, and finally Iglesias-Juez et al. [18] reported 12.5%.

#### 2.2.4. Effect of $H_2O$ on $H_2$–$C_3H_8$–SCR of NO

The effect of water in this reaction was studied with the catalyst 2 wt%Ag/γ-$Al_2O_3$ [50] by adding 6%vol. $H_2O$. It was found that the addition of $H_2O$ decreased the NO conversion (9% on average) at 150 °C compared to the NO conversion without $H_2O$, but increased it (8.4% on average) in the temperature range of 200 to 360 °C. The opposite happened with the $C_3H_8$ conversion. In this case, the addition of $H_2O$ improved the conversion (6% on average) compared with the $C_3H_8$ conversion without $H_2O$ in the range of 250 to 450 °C.

The presence of water vapor could decrease the concentration of carbonaceous deposits that block adsorption sites on the catalyst surface [2], which could largely explain the increase in $C_3H_8$ conversion. The authors studied the SCR of NO with 10 vol.%$H_2O$ on an $In_2O_3$/$Ga_2O_3$/$Al_2O_3$ catalyst. The authors mentioned that the presence of water vapor partially inhibited the non-selective combustion of $C_3H_8$ with $O_2$. As a result, more hydrocarbons could be available for the SCR reaction resulting in increased activity and selectivity for this reaction.

This behavior has already been reported when small hydrocarbons such as $C_3H_8$ react. It has been mentioned that one possible reason is the lower enthalpy of adsorption of the short alkanes compared to the large chain alkanes.

## 3. Materials and Methods

### 3.1. Preparation of Catalysts

The synthesis of $Al_2O_3$ (A) was carried out by the precipitation of a 0.44 mg/mL solution of $Al(NO_3)_3 \cdot 9H_2O$ (Fermont, Mexico) to which a solution of $NH_4OH$ at 30 vol.% was added dropwise (JT Baker, USA) under stirring, until a boehmite suspension with a pH of 9–10 was obtained, which was left to stand for 12 h. The solid was filtered, dried at 110 °C for 24 h, and then calcined at 500 °C for 6 h.

The catalyst containing 0.4 wt%Pt/$Al_2O_3$ (0.4Pt/A) was prepared by the incipient wetness impregnation method using 52.8 mL of an $H_2PtCl_6$ solution (Aldrich, USA) with a concentration of 0.38 mgPt/mL on 5 g of $Al_2O_3$. The impregnation started with a pH of 2.5 at 60 °C for 2 h, then dried at 110 °C for 12 h, and finally calcined at 500 °C for 6 h.

The synthesis of the $Al_2O_3$ support promoted with WOx(AW) was carried out with the same procedure as the $Al_2O_3$ (A) synthesis by adding the required amount of $(NH_4)_{12}W_{12}O_{40}\cdot 5H_2O$ (Aldrich, USA) to obtain a nominal content of 0.5 wt%W during precipitation.

The 0.4 wt%Pt/$Al_2O_3$–WOx (0.4Pt/AW) catalyst was prepared using the same $H_2PtCl_6$ incipient wetness impregnation method used in the 0.4Pt/$Al_2O_3$ catalyst.

The 2 wt%Ag/$Al_2O_3$–WOx (2Ag/AW) catalyst was also obtained by impregnation by the incipient wetness method using 25 mL of a $AgNO_3$ solution (Aldrich, USA) containing 4 mgAg/mL on 5 g of $Al_2O_3$–WOx (AW) at 60 °C for 2 h. The solid was dried at 110 °C for 12 h and finally calcined in air at 500 °C for 6 h.

The Pt–Ag/$Al_2O_3$–WOx (PtAg/AW) bimetallic catalysts were prepared with the same incipient wetness impregnation method used for the preparation of 0.4Pt/AW and 2Ag/AW monometallic catalysts; however, they were impregnated sequentially, starting with the impregnation of Pt and then the Ag to achieve strong contact between the two metals [53]. During the impregnation, 13.15, 32.89, 52.8, and 131.56 mL of $H_2PtCl_6$ solution in 5 g of $Al_2O_3$-WOx (pH = 2.5) were used to obtain solids with a Pt content of 0.1, 0.25, 0.4, and 1 wt% Pt, respectively. The solids were dried at 110 °C for 12 h and calcined at 500 °C for 6 h. Subsequently, 5 g of the calcined solids were impregnated with 25 mL of a solution of $AgNO_3$ (4 mgAg/mL) (Aldrich, USA) to obtain a concentration of 2 wt%Ag. This solution was soaked at 60 °C for 2 h, dried at 110 °C for 12 h, and calcined at 500 °C for 6 h. All catalysts were reduced in $H_2$ flow (30 $cm^3$/min) at 500 °C for 2 h.

### *3.2. Catalyst Characterization*

The catalysts were characterized by adsorption-desorption of $N_2$. The measurement of the isotherms was carried out on ASAP-2460 Version 2.01 (Micromeritics, Norcross, GA, USA) equipment. The samples received pretreatment in a vacuum ($1 \times 10^{-4}$ Torr) at 300 °C for 14 h; after that, physisorption with $N_2$ was performed at −196 °C (77 K). The BET and BJH methods were used to determine the specific area, diameter, and pore volume.

The crystalline phases were obtained in a Bruker diffractometer (D8FOCUS) (Bruker, Karlsruhe, Germany) operated at 35 kV and 25 mA using Cu $K\alpha$ radiation ($\lambda$ = 0.154 nm) at a goniometer speed of 2°/min with a sweep of $10° \leq 2\theta \leq 100°$. A special detector called "Lynx Eyes" was used. The identification of the different crystalline phases was compared with the data from the corresponding JCPDS diffraction cards.

Temperature programmed reduction (TPR) profiles of the calcined Pt/$Al_2O_3$ samples were obtained under $H_2$ flow (10 vol.%$H_2$/Ar) by using a commercial thermodesorption apparatus (multipulse RIG model, from ISRI) equipped with a thermal conductivity detector (TCD). Samples of 30 mg and a gas flow rate of 25 $cm^3$/min were used in the experiments. The TPR profiles were registered by heating the sample from 25 to 600 °C at a rate of 10 °C/min, and a TCD monitored the rate of $H_2$ consumption. The amount of $H_2$ consumed was obtained by the deconvolution and integration of the TPR peaks using the Peak Fit program. The calibration was done by measuring the change in weight due to a reduction in $H_2$ of 2 mg of CuO using an electrobalance Cahn-RG. The TPR signal of CuO was made and correlated with the stoichiometric $H_2$ consumption.

Chemisorption measurements of $H_2$ were performed using a conventional volumetric glass apparatus (base pressure $1 \times 10^{-5}$ Torr). The amount of chemisorbed $H_2$ was determined from adsorption isotherms measured at room temperature (25 °C). In a typical experiment, the catalysts (0.5 g) were reduced in $H_2$ at 500 °C for 1 h, then evacuated at the same temperature for 2 h and cooled down under vacuum to 25 °C. After that, the first adsorption isotherm was measured. The catalyst was then evacuated to $1 \times 10^{-5}$ Torr for 30 min at 25 °C to remove the physisorbed species and back-sorption isotherm. The linear parts of the isotherms were extrapolated to zero pressure. The subtraction of the two isotherms gave the amount of $H_2$ strongly chemisorbed on metal particles. These values were then used to calculate the Pt dispersion (H/Pt ratio). In preliminary experiments, it was found that chemisorptions of hydrogen on the $Al_2O_3$ support were negligible at 25 °C. The uncertainty of the reported uptakes was ±0.45 μmol $H_2/g_{cat}$.

The materials' microstructure images were taken by scanning electron microscopy (SEM) with field emission and high resolution in a Joel microscope (model JFM-6701-F) (JEOL Ltd., Tokyo, Japan) using secondary electrons. The qualitative and quantitative chemical analyses and their corresponding images were obtained by attaching an x-ray energy dispersion spectroscopy (EDS) probe to the microscope.

Ex situ UV–Visible spectra of the powder samples calcined at 500 °C were obtained with a UV–Vis spectrophotometer (GBC model Cintra 20) (GBC Scientific Equipment, Braeside, Australia) with a wavelength of 200 to 800 nm under ambient conditions.

In situ UV–Visible spectra of the powder 0.4Pt/AW catalyst calcined at 500 °C were collected using an Agilent Cary 5000 spectrometer (Agilent Technologies Inc., Santa Clara, CA, USA) equipped with a Harrick Praying Mantis. During the experiment, 50 mg of the sample was packed in the sample holder. The spectra were recorded in the range of 200–1000 nm with a resolution of 0.1 nm each 100 °C from 25 to 500 °C in a gas mixture of 5 vol.%$H_2/N_2$, with a flow of 0.5 $cm^3$/s.

### 3.3. Catalytic Evaluation

The catalytic activity for $C_3H_8$–SCR was carried out in a quartz microreactor with a diameter of 10 mm, which was operated under kinetic conditions where the phenomena of mass transfer by internal and external diffusion were minimized, for which the value of the Weisz and Prater criterion was calculated [63–65] (Supplementary Material SI.2).

The effect of the reducing agent, $H_2$, was investigated at a gas hourly space velocity (GHSV) of 128,000 $h^{-1}$. The flow used was 400 $cm^3$/min and a sample of 150 mg was placed (100 US mesh, 0.148 mm). Prior to each test, the samples were pretreated in a flow of 20 $cm^3$/min with a mixture containing 13.2 vol.% $H_2$ with $N_2$ at 500 °C for 2 h.

The temperature of reaction increased from 50 to 600 °C at 5 °C/min. The feed mixture to the microreactor was: 500 ppm of NO, 625 ppm of $C_3H_8$, 200 ppm of CO, 660 ppm of $H_2$, 2 vol.%$O_2$, and $N_2$ (balance). The pure gases were chromatographic grade $O_2$, $H_2$, and $N_2$ (99.90% Infra S.A.) and a prepared mixture of NO, CO, and propane (Praxair, USA). The concentration of the gases in the feed to the microreactor varied according to the reaction experiment ($C_3H_8$–SCR or $H_2$–$C_3H_8$–SCR). The gas flows were controlled by mass flow controllers (AALBORG, Repeatability: ±0.25% of full scale) and the inlet and outlet gas composition was analyzed as described below.

The $C_3H_8$ was analyzed in a gas chromatograph (Gow-Mac, 550, GOW-MAC Instrument Company, Bethlehem, PA, USA) with a flame ionization detector and six feet packed column using a stationary phase, tri-cresyl phosphate in bentonite-34. The analysis of NO and $NO_2$ was performed by chemiluminescence with a Rosemount Analytical analyzer (Model 951A NO/NOx Analyzer, Rosemount Analytical Inc., Anaheim, CA, USA). The $N_2O$ was analyzed in another gas chromatograph (Gow-Mac, 580) with a thermal conductivity detector using He as the carrier gas (52 $cm^3$/min) with a 10 feet packed column of Porapak Q at a temperature of 50 °C (note that this column can also analyze air, NO, $NO_2$, $N_2O$, $CO_2$ and $H_2O$). Bridge current: 150 mA, Response time: 0.5 s, noise: 10 μVmax. (within operating parameters), drift: 40 μV/hour max. The repeatability of the experiments carried out was 0.71, which means that it represents a moderate repeatability in the measurement of experiments according to David G.C. [66], and the absolute error of ±5 ppm $N_2O$. The average retention times were: 0.62 min (Air), 0.75 min (NO), 1.1 min ($NO_2$), 2.1 min ($CO_2$), 2.75 min ($N_2O$), and 8.25 min ($H_2O$). The analysis of CO and $H_2$ was made in a Gow-Mac, 580 gas chromatograph with a TCD detector using He as the carrier gas and a 13× molecular sieve packed column (1/8 in × 8 ft).

The experiments of the combustion of $C_3H_8$ (see Supplementary Material SI.1 and Appendix A) were made in a flow microreactor connected in-line to a gas chromatograph (Gow-Mac, 550) with a flame ionization detector and six feet packed column using a stationary phase, tri-cresyl phosphate in bentonite-34. The propane composition was 999 ppm in dry air (Linde). The total pressure within the reaction system remained constant at 590 Torr and the gas flow used in all of the experiments was

300 $cm^3$/min. The amounts of catalyst evaluated were 20 mg. The samples were evaluated by scanning temperatures from room temperature to 500 °C at a fixed time of 90 min. The deactivation tests were carried out at the same final temperature and for 180 min, keeping all other variables constant.

The equations to calculate the conversion of NO(X) and the yield to a product (Yi) are as follows:

$$X = ([NO]_o - [NO])/[NO]_o) \times 100 \tag{2}$$

$$Y_{N2O} = 2 \times [N_2O]/[NO]_o \times 100 \tag{3}$$

## 4. Conclusions

The addition of 0.1 wt%Pt to the 2 wt%Ag/$Al_2O_3$–WOx catalyst improved the $C_3H_8$–SCR of NO assisted by $H_2$ and widened the range of conversions with respect to the reaction temperature.

Bimetallic PtAg particles were formed, having a strong contact between the metals, and had the capacity of adsorbing $H_2$. Pt dispersion was more significant in the particles with a lower concentration of Pt, and the Ag monometallic catalyst did not show $H_2$ chemisorption.

After reduction with $H_2$, Ag and PtAg particles were obtained in all the bimetallic catalysts. It appears that the bimetallic PtAg particles have adsorption properties that explain the differences with the Ag/$Al_2O_3$ catalysts.

Utilizing ex situ UV–Vis spectroscopy, species such as $Ag^+$ and $Ag_n^{\delta+}$ were found as well as $Ag^0$ nanoparticles after SCR of NO with $C_3H_8$ and $H_2$ in a wide temperature range. By SEM, mainly spherical clusters of small particles of less than 10 nm were found in the calcined Pt catalyst, which was probably related to the presence of $Ag_2O$. The distribution of particle diameters indicated the predominance (31.64%) of particles of 10 nm or less.

The $C_3H_8$–SCR of NO from the PtAg/$Al_2O_3$ bimetallic catalysts promoted with WOx was considerably improved by adding $H_2$ to the combustion gases due to the formation of Ag clusters, (or PtAg clusters), enolic species, and the decrease in nitrate self-poisoning, which is a stage before the formation of N-containing species.

The addition of 0.5 wt%W to the $Al_2O_3$ and the Pt/$Al_2O_3$-WOx catalysts stabilized them in the propane combustion reaction.

**Supplementary Materials:** The following are available online at http://www.mdpi.com/2073-4344/10/10/1212/s1, Figure S1: $C_3H_8$ combustion in air over the (•) 0.4Pt/A; (□) 0.4Pt/AW catalysts reduced to 500 and 800°C. (**a**) Effect of reduction temperature on catalyst 0.4Pt/A without W; (**b**) Effect of reduction temperature on catalyst 0.4Pt/AW with W; (**c**) Effect of WOx during catalyst deactivation 0.4Pt/A without W and 0.4Pt/AW with W reduced to 500°C and (**d**) Effect of WOx during deactivation of 0.4Pt/A catalysts without W and 0.4Pt/AW with W reduced to 800°C. Evaluation conditions: 300$cm^3$/min of air mixture flow plus 999 ppm of $C_3H_8$, catalyst weight: 20 mg, Table S1: Microreactor operating conditions to evaluate the SCR of NO at 250°C (average temperature).

**Author Contributions:** Conceptualization, J.L.C., G.A.F., N.N.G.H., M.E.H.-T., and M.P.; Methodology, J.L.C., N.N.G.H., and M.P.; Investigation, G.A.F., N.N.G.H., and M.P.; Resources, J.L.C., B.Z., J.L.F.M., T.V., and J.M.J.; Data curation, J.L.C.; Writing-preparing the initial draft, N.N.G.H.; Critical writing-review and editing, J.L.C., J.S., and B.Z.; Visualization, N.N.G.H.; Supervision, J.L.C.; Project administration, J.L.C.; Procurement of funds, J.L.C. All authors have read and agreed to the published version of the manuscript.

**Funding:** This research received no external funding.

**Acknowledgments:** Naomi N. González Hernández thanks CONACYT for the postgraduate scholarship awarded through program 001379. We thank the Catalysis Laboratory, UAM-A, and the Chemical Industry Process Laboratory, UAM-A., J.L. Contreras appreciates the support of the company Synthesis and Industrial Applications, S.A.

**Conflicts of Interest:** The authors declare no conflict of interest.

## Appendix A. Stabilization of $Al_2O_3$ and Pt/$Al_2O_3$ Catalysts

The addition of tungsten oxides (WOx) to the $Al_2O_3$ support means that at low concentrations of W (0.5 wt%W), it is possible to thermally stabilize the $Al_2O_3$ structure at high temperatures (600 to 900 °C), as can be seen in Figure A1. The BET area of the $Al_2O_3$ samples calcined at 650, 800, and 950 °C was higher when more than 0.5 wt% of W was added. In other words, W acts as a structural promoter of $Al_2O_3$, allowing the $Ag/Al_2O_3$ catalyst to more extensively withstand the inevitable thermal sintering at high temperatures during reactions.

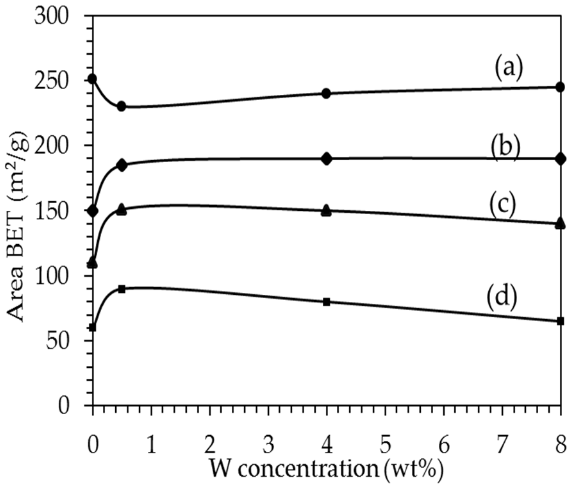


**Figure A1.** BET area against W concentration (in wt%W) named $Al_2O_3$–WOx, when the calcination temperature increased: (**a**) 500 °C; (**b**) 650 °C; (**c**) 800 °C; (**d**) 950 °C for 6 h.

On the other hand, we studied the effect of the W/Pt ratio on the Pt's dispersion for catalysts supported in $Al_2O_3$ [44,45] when they were subjected to reduction in $H_2$ at 500 °C and 800 °C (Figure A2). It was observed that the catalyst reduced to 800 °C without W (ratio W/Pt = 0) showed a dispersion of 42%, while the catalyst with a W/Pt ratio of 3.28 showed a dispersion of 60%.

However, as Figure A2 shows, as the W/Pt ratio increases, the dispersion of Pt decreases, and it can be observed that this trend is more pronounced in samples reduced to 500 °C than in samples reduced to 800 °C. This behavior suggests that the presence of WOx in the presence of PtOxCly could inhibit the formation of metallic Pt because a higher reduction temperature (800 °C) would be required to obtain a better dispersion of Pt.

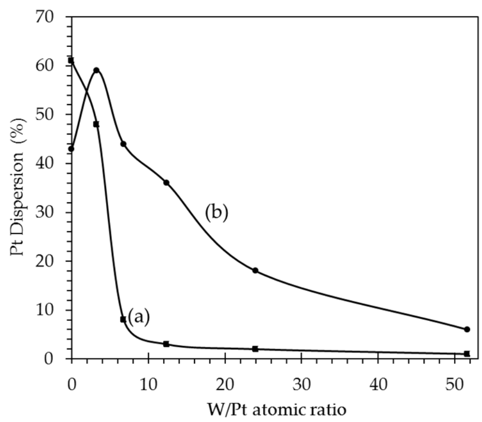


**Figure A2.** Dispersion of Pt in Pt/AW catalysts increasing the W/Pt atomic ratio when the reduction temperature in $H_2$ increased from (**a**) 500 to (**b**) 800 °C (for 4 h).

## References


1. Twigg, M.V. Progress and future challenges in controlling automotive exhaust gas emissions. *Appl. Catal. B Environ.* **2007**, *70*, 2–15. [CrossRef]
2. Burch, R.; Breen, J.P.; Meunier, F.C. A review of the selective reduction of NOx with hydrocarbons under lean-burn conditions with non-zeolitic oxide and platinum group metal catalysts. *Appl. Catal. B Environ.* **2002**, *39*, 283–303. [CrossRef]
3. Kannisto, H.; Ingelsten, H.H.; Skoglundh, M. Ag–$Al_2O_3$ catalysts for lean NOx reduction—Influence of preparation method and reductant. *J. Mol. Catal. A Chem.* **2009**, *302*, 86–96. [CrossRef]
4. Nakatsuji, T.; Yasukawa, R.; Tabata, K.; Ueda, K.; Niwa, M. Catalytic reduction system of NOx in exhaust gases from diesel engines with secondary fuel injection. *Appl. Catal. B Environ.* **1998**, *17*, 333–345. [CrossRef]
5. Miyadera, T.; Yoshida, K. Alumina-supported catalysts for the selective reduction of nitric oxide by propene. *Chem. Lett.* **1993**, *9*, 1483–1486. [CrossRef]
6. Satokawa, S.; Yamaseki, K.; Uchida, H. Influence of low concentration of $SO_2$ for selective reduction of NO by $C_3H_8$ in lean-exhaust conditions on the activity of Ag/$Al_2O_3$ catalyst. *Appl. Catal. B Environ.* **2001**, *34*, 299–306. [CrossRef]
7. Kyriienko, P.; Popovych, N.; Soloviev, S.; Orlyk, S.; Dzwigaj, S. Remarkable activity of Ag/$Al_2O_3$/cordierite catalysts in SCR of NO with ethanol and butanol. *Appl. Catal. B Environ.* **2013**, *140–141*, 691–699. [CrossRef]
8. Popovych, N.O.; Soloviev, S.O.; Orlyk, S.M. Selective reduction of nitrogen oxides (NOx) with oxygenates and hydrocarbons over bifunctional, silver–alumina catalysts: A review. *Theor. Exp. Chem.* **2016**, *52*, 133–151. [CrossRef]
9. Männikkö, M.; Wang, X.; Skoglundh, M.; Härelind, H. Characterization of the active species in the silver/alumina system for lean NOx reduction with methanol. *Catal. Today* **2016**, *267*, 76–81. [CrossRef]
10. Deng, H.; Yu, Y.; He, H. Adsorption states of typical intermediates on Ag/$Al_2O_3$ catalyst employed in the selective catalytic reduction of NOx by ethanol. *Chin. J. Catal.* **2015**, *36*, 1312–1320. [CrossRef]
11. Bethke, K.A.; Kung, H.H. Supported Ag catalysts for the lean reduction of NO with $C_3H_6$. *J. Catal.* **1997**, *172*, 93–102. [CrossRef]
12. Hoost, T.E.; Kudla, R.J.; Collins, K.M.; Chattha, M.S. Characterization of Ag/$\gamma$-$Al_2O_3$ catalysts and their lean-NOx properties. *Appl. Catal. B Environ.* **1997**, *13*, 59–67. [CrossRef]
13. Kung, M.C.; Kung, H.H. Lean NOx catalysis over alumina-supported catalysts. *Top. Catal.* **2000**, *10*, 21–26. [CrossRef]
14. Meunier, F.C.; Breen, J.P.; Zuzaniuk, V.; Olsson, M.; Ross, J.R.H. Mechanistic aspects of the selective reduction of NO by propene over alumina and silver-alumina catalysts. *J. Catal.* **1999**, *187*, 493–505. [CrossRef]
15. Martínez-Arias, A.; Fernández-García, M.; Iglesias-Juez, A.; Anderson, J.A.; Conesa, J.C.; Soria, J. Study of the lean NOx reduction with $C_3H_6$ in the presence of water over silver/alumina catalysts prepared from inverse microemulsions. *Appl. Catal. B Environ.* **2000**, *28*, 29–41. [CrossRef]
16. Shimizu, K.I.; Shibata, J.; Yoshida, H.; Satsuma, A.; Hattori, T. Silver-alumina catalysts for selective reduction of NO by higher hydrocarbons: Structure of active sites and reaction mechanism. *Appl. Catal. B Environ.* **2001**, *30*, 151–162. [CrossRef]
17. Bogdanchikova, N.; Meunier, F.C.; Avalos-Borja, M.; Breen, J.P.; Pestryakov, A. On the nature of the silver phases of Ag/$Al_2O_3$ catalysts for reactions involving nitric oxide. *Appl. Catal. B Environ.* **2002**, *36*, 287–297. [CrossRef]
18. Iglesias-Juez, A.; Hungría, A.B.; Martínez-Arias, A.; Fuerte, A.; Fernández-García, M.; Anderson, J.A. Nature and catalytic role of active silver species in the lean NOx reduction with $C_3H_6$ in the presence of water. *J. Catal.* **2003**, *217*, 310–323. [CrossRef]
19. Arve, K.; Capek, L.; Klingstedt, F.; Eränen, K.; Lindfors, L.E.; Murzin, D.Y. Preparation and characterization of Ag/alumina catalysts for the removal of NOx emissions under oxygen rich conditions. *Top. Catal.* **2004**, *30*, 91–95. [CrossRef]
20. Mrabet, D.; Manh-Hiep, V.; Kaliaguine, S.; Trong-On, D. A new route to the shape-controlled synthesis of nano-sized $\gamma$-alumina and Ag/$\gamma$-alumina for selective catalytic reduction of NO in the presence of propene. *J. Colloid Interface Sci.* **2017**, *485*, 144–151. [CrossRef]
21. Keshavaraja, A.; She, X.; Flytzani-Stephanopoulos, M. Selective catalytic reduction of NO with methane over Ag-alumina catalysts. *Appl. Catal. B Environ.* **2000**, *27*, L1–L9. [CrossRef]

22. Shimizu, K.; Satsuma, A.; Hattori, T. Catalytic performance of Ag–$Al_2O_3$ catalyst for the selective catalytic reduction of NO by higher hydrocarbons. *Appl. Catal. B Environ.* **2000**, *25*, 239–247. [CrossRef]
23. She, X.; Flytzani-Stephanopoulos, M. The role of Ag–O–Al species in silver–alumina catalysts for the selective catalytic reduction of NOx with methane. *J. Catal.* **2006**, *237*, 79–93. [CrossRef]
24. Luo, Y.; Hao, J.; Hou, Z.; Fu, L.; Li, R.; Ning, P.; Zheng, X. Influence of preparation methods on selective catalytic reduction of nitric oxides by propene over silver–alumina catalyst. *Catal. Today* **2004**, *93–95*, 797–803. [CrossRef]
25. Chaieb, T.; Delannoy, L.; Costentin, G.; Louis, C.; Casale, S.; Chantry, R.L.; Li, Z.Y.; Thomas, C. Insights into the influence of the Ag loading on $Al_2O_3$ in the $H_2$-assisted $C_3H_6$-SCR of NOx. *Appl. Catal. B Environ.* **2014**, *156–157*, 192–201. [CrossRef]
26. Tamm, S.; Vallim, N.; Skoglundh, M.; Olsson, L. The influence of hydrogen on the stability of nitrates during $H_2$-assisted SCR over Ag/$Al_2O_3$ catalysts—A DRIFT study. *J. Catal.* **2013**, *307*, 153–161. [CrossRef]
27. Azis, M.M.; Härelind, H.; Creaser, D. On the role of $H_2$ to modify surface NOx species, over Ag–$Al_2O_3$ as lean NOx reduction catalyst: TPD and DRIFTS studies. *Catal. Sci. Technol.* **2015**, *5*, 296–309. [CrossRef]
28. Azis, M.M.; Härelind, H.; Creaser, D. Kinetic modeling of $H_2$-assisted $C_3H_6$ selective catalytic reduction of NO over silver alumina catalyst. *Chem. Eng. J.* **2015**, *278*, 394–406. [CrossRef]
29. Singh, P.; Yadav, D.; Thakur, P.; Pandey, J.; Prasad, R. Studies on $H_2$-Assisted Liquefied Petroleum Gas Reduction of NO over Ag/$Al_2O_3$ Catalyst. *Bull. Chem. React. Eng. Catal.* **2018**, *13*, 227–235.
30. Hernández-Terán, M.E.; Fuentes, G.A. Enhancement by $H_2$ of $C_3H_8$-SCR of NOx using Ag/γ-$Al_2O_3$. *Fuel* **2014**, *138*, 91–97. [CrossRef]
31. Ström, L.; Carlsson, P.-A.; Skoglundh, M.; Härelind, H. Surface Species and Metal Oxidation State during $H_2$-Assisted $NH_3$-SCR of NOx over Alumina-Supported Silver and Indium. *Catalysts* **2018**, *8*, 38. [CrossRef]
32. Xu, G.; Ma, J.; Wang, L.; Lv, Z.; Wang, S.; Yu, Y.; He, H. Mechanism of the $H_2$ Effect on $NH_3$-Selective Catalytic Reduction over Ag/$Al_2O_3$: Kinetic and Diffuse Reflectance Infrared Fourier Transform Spectroscopy Studies. *ACS Catal.* **2019**, *9*, 10489–10498. [CrossRef]
33. Barreau, M.; Tarot, M.-L.; Duprez, D.; Courtois, X.; Can, F. Remarkable enhancement of the selective catalytic reduction of NO at low temperature by collaborative effect of ethanol and $NH_3$ over silver supported catalyst. *Appl. Catal. B Environ.* **2018**, *220*, 19–30. [CrossRef]
34. Pihl, J.A.; Toops, T.J.; Fisher, G.B.; West, B.H. Selective catalytic reduction of nitric oxide with ethanol/gasoline blends over a silver/alumina catalyst. *Catal. Today* **2014**, *231*, 46–55. [CrossRef]
35. Wu, S.; Li, X.; Fang, X.; Sun, Y.; Sun, J.; Zhou, M.; Zang, S. NO reduction by CO over $TiO_2$-γ-$Al_2O_3$ supported In/Ag catalyst under lean burn conditions. *Chin. J. Catal.* **2016**, *37*, 2018–2024. [CrossRef]
36. Shang, Z.; Cao, J.; Wang, L.; Guo, Y.; Lu, G.; Guo, Y. The study of $C_3H_8$-SCR on Ag/$Al_2O_3$ catalysts with the presence of CO. *Catal. Today* **2017**, *281*, 605–660. [CrossRef]
37. Gunnarsson, F.; Kannisto, H.; Skoglundh, M.; Härelind, H. Improved low-temperature activity of silver–alumina for lean NOx reduction—Effects of Ag loading and low-level Pt doping. *Appl. Catal. B Environ.* **2014**, *152–153*, 218–225. [CrossRef]
38. Tamm, S.; Andonova, S.; Olsson, L. The Effect of Hydrogen on the Storage of NOx over Silver, Platinum and Barium Containing NSR Catalysts. *Catal. Lett.* **2014**, *144*, 1101–1112. [CrossRef]
39. Bonet, F.; Grugeon, S.; Herrera Urbina, R.H.; Tekaia-Elhsissen, K.; Tarascon, J.-M. In situ deposition of silver and palladium nanoparticles prepared by the polyol process and their performance as catalytic converters of automobile exhaust gases. *Solid State Sci.* **2002**, *4*, 665–670. [CrossRef]
40. He, H.; Wang, J.; Feng, Q.; Yu, Y.; Yoshida, K. Novel Pd, promoted Ag/$Al_2O_3$ catalyst for the selective reduction of NOx. *Appl. Catal. B Environ.* **2003**, *46*, 365–370. [CrossRef]
41. Inderwildi, O.R.; Jenkins, S.J.; King, D.A. When adding an unreactive metal enhances catalytic activity: NOx decomposition over silver–rhodium bimetallic surfaces. *Surf. Sci.* **2007**, *601*, L103–L108. [CrossRef]
42. Lanza, R.; Eriksson, E.; Pettersson, L.J. NOx selective catalytic reduction over supported metallic catalysts. *Catal. Today* **2009**, *147S*, S279–S284. [CrossRef]
43. Schott, F.J.P.; Balle, P.; Adler, J.; Kureti, S. Reduction of NOx by $H_2$ on Pt/$WO_3$/$ZrO_2$ catalysts in oxygen-rich exhaust. *Appl. Catal. B Environ.* **2009**, *87*, 18–29. [CrossRef]

44. Contreras, J.L.; Fuentes, G.A.; García, L.A.; Salmones, J.; Zeifert, B. WOx effect on the catalytic properties of Pt particles on $Al_2O_3$. *J. Alloy Compd.* **2009**, *483*, 450–452. [CrossRef]
45. Contreras, J.L.; Fuentes, G.A.; Zeifert, B.; García, L.A.; Salmones, J. Stabilization of Supported Platinum Nanoparticles on γ-Alumina Catalysts by Addition of Tungsten. *J. Alloy Compd.* **2009**, *483*, 371–373. [CrossRef]
46. Muñoz, H.P.; Delmás, R.D. Alumina synthesis from $AlCl_3$ acid solution and XRD characterization. *J. Per. Quim. Ing. Química* **2001**, *4*, 68–71.
47. Aguado, J.; Escola, J.M.; Castro, M.C. Influence of the thermal treatment upon the textural properties of sol–gel mesoporous γ-alumina synthesized with cationic surfactants. *Microporous Mesoporous Mater.* **2010**, *128*, 48–55. [CrossRef]
48. Richter, M.; Bentrup, U.; Eckelt, R.; Schneider, M.; Pohl, M.M.; Fricke, R. The effect of hydrogen on the selective catalytic reduction of NO in excess oxygen over $Ag/Al_2O_3$. *Appl. Catal. B Environ.* **2004**, *51*, 261–274. [CrossRef]
49. Vojvodic, A.; Calle-Vallejo, F.; Guo, W.; Wang, S.; Toftelund, A.; Studt, F.; Martínez, J.I.; Shen, J.; Man, J.; Rossmeisl, I.C.; et al. On the behavior of Brønsted-Evans-Polanyi relations for transition metal oxides. *J. Chem. Phys.* **2011**, *134*, 244–509. [CrossRef]
50. Hernández-Terán, M.E. Development of Ag/γ-$Al_2O_3$ and Ag/η-$Al_2O_3$ Catalytic Systems for $H_2$-Assisted NO $C_3H_8$-SCR under Oxidizing Operation for Emission Control Systems for Diesel Engines or Stationary Sources. Ph.D. Thesis, Universidad Autónoma Metropolitana-Iztapalapa, Ciudad de México, Mexico, 2020.
51. Zhang, Q.; Li, J.; Liu, X.; Zhu, Q. Synergetic effect of Pd and Ag dispersed on $Al_2O_3$ in the selective hydrogenation of acetylene. *Appl. Catal. A General* **2000**, *197*, 221–228. [CrossRef]
52. Lieske, H.; Lietz, G.; Spindler, H.; Volter, J. Reactions of Platinum in Oxygen- and Hydrogen-Treated Pt/$A1_20_3$ Catalysts. Temperature-Programmed Reduction, Adsorption, and Redispersion of Platinum. *J. Catal.* **1983**, *81*, 8–16.
53. Gauthard, F.; Epron, F.; Barbier, J. Palladium and platinum-based catalysts in the catalytic reduction of nitrate in water: Effect of cooper, silver or gold addition. *J. Catal.* **2003**, *220*, 182–191. [CrossRef]
54. De Jong, K.P.; Bongenaar-Schlenter, B.E.; Meima, G.R.; Verkerk, R.C.; Lammers, M.J.J.; Geus, J.W. Investigations on silica-supported platinum-silver alloy particles by infrared spectra of adsorbed CO and $N_2$. *J. Catal.* **1983**, *81*, 67–76. [CrossRef]
55. Prasad, J.; Murthy, K.R.; Menon, P.G. The stoichiometry of hydrogen-oxygen titrations on supported platinum catalysts. *J. Catal.* **1978**, *52*, 515–520. [CrossRef]
56. Arve, K.; Svennerberg, K.; Klingstedt, F.; Eranen, K.; Wallenberg, L.R.; Bovin, J.O.; Capek, L.; Murzin, D.Y. Structure-Activity Relationship in HC-SCR of NOx by TEM, $O_2$-Chemisorption, and EDXS Study of $Ag/Al_2O_3$. *J. Phys. Chem. B* **2006**, *110*, 420–427. [CrossRef]
57. Bligaard, T.; Nørskov, J.K.; Dahl, S.; Matthiesen, J.; Christensen, C.H.; Sehested, J. The Brønsted–Evans–Polanyi relation and the volcano curve in heterogeneous catalysis. *J. Catal.* **2004**, *224*, 206–217. [CrossRef]
58. Lietz, G.; Lieske, H.; Spindler, H.; Hanke, W.; Völter, J. Reactions of Platinum in Oxygen- and Hydrogen-Treated Pt/γ-$Al_2O_3$ catalysts, II. Ultraviolet-Visible Studies, Sintering of Platinum, and Soluble Platinum. *J. Catal.* **1983**, *81*, 17–25. [CrossRef]
59. Barton, D.G.; Soled, S.L.; Meitzner, G.D.; Fuentes, G.A.; Iglesia, E. Structural and Catalytic Characterization of Solid Acids Based on Zirconia Modified by Tungsten Oxide. *J. Catal.* **1999**, *181*, 57–72. [CrossRef]
60. Satokawa, S. Enhancing the $NO/C_3H_8/O_2$ Reaction by Using $H_2$ over $Ag/Al_2O_3$ Catalysts under Lean-Exhaust Conditions. *Chem. Lett.* **2000**, *29*, 294–295. [CrossRef]
61. Wang, J.; He, H.; Feng, Q.; Yu, Y.; Yoshida, K. Selective catalytic reduction of NOx with $C_3H_6$ over $Ag/Al_2O_3$ catalyst with a small quantity of noble metal. *Catal. Today* **2004**, *93–95*, 783–789. [CrossRef]
62. Bordley, J.A.; El-Sayed, M.A. Enhanced Electrocatalytic Activity toward the Oxygen Reduction Reaction through Alloy Formation: Platinum-Silver Alloy Nano cages. *J. Phys. Chem.* **2016**, *120*, 14643–14651. [CrossRef]
63. Fogler, S.H. *Elements of Chemical Reaction Engineering*, 3rd ed.; Prentice Hall Inc.: Upper Saddle River, NJ, USA, 1999; pp. 738–758.
64. Smith, J.F. *Chemical Engineering Kinetics*, 3rd ed.; McGraw-Hill Inc.: New York, NY, USA, 1986; pp. 524–534.

65. Hirshfelder, J.O.; Curtis, C.F.; Bird, R.B. *Molecular Theory of Gases and Liquids*, 1st ed.; Wiley: Hoboken, NJ, USA, 1964; ISBN 0-471-40065-3.
66. David, G.C. Some comments on the repeatability of measurements. *Ringing Migr.* **1994**, *15*, 84–90.